Numerical analysis of natural convection in a differentially heated packed bed with non-uniform wall temperature

Chakkingal, Manu; Kenjereš, Saša; Dadavi, Iman Ataei; Tummers, M. J.; Kleijn, Chris R.

DOI
10.1016/j.ijheatmasstransfer.2019.119168

Publication date
2020

Document Version
Final published version

Published in
International Journal of Heat and Mass Transfer

International Journal of Heat and Mass Transfer 149 (2019) 119168

Contents lists available at ScienceDirect

International Journal of Heat and Mass Transfer

journal homepage: www.elsevier.com/locate/hmt

Numerical analysis of natural convection in a differentially heated packed bed with non-uniform wall temperature

Manu Chakkingal[a,*], Saša Kenjereš[a], Iman Ataei Dadavi[a], M.J. Tummers[b], Chris R. Kleijn[a]

[a] Transport Phenomena Section, Department of Chemical Engineering, Delft University of Technology, Delft, the Netherlands
[b] Fluid Mechanics Section, Department of Process and Energy, Delft University of Technology, Delft, the Netherlands

ARTICLE INFO

Article history:
Received 11 October 2019
Revised 26 November 2019
Accepted 3 December 2019

Keywords:
Natural convection
Side heated cavity
Porous-media
Steady-state
Local flow and heat transfer
Non-uniform wall temperature
Entropy generation
OpenFOAM

ABSTRACT

We report numerical simulations of natural convection and conjugate heat transfer in a differentially heated cubical cavity packed with relatively large hydrogel beads ($d/L = 0.2$) in a Simple Cubic Packing configuration. We study the influence of a spatially non-uniform, sinusoidally varying, wall temperature on the local flow and heat transfer, for a solid-to-fluid conductivity ratio of 1, a fluid Prandtl number of 5.4, and fluid Rayleigh numbers between 10^5 and 10^7. We present local and overall flow and heat transfer results for both sphere packed and water-only filled cavities, when subjected to variations of the wall temperature at various combinations of the amplitude and characteristic phase angle of the imposed wall temperature variations. It is found that imposing a sinusoidal spatial variation in the wall temperature may significantly alter the local flow and heat transfer, and consequently the overall heat transfer. At identical average temperature difference, applying a spatial variation in wall temperature at well-chosen phase angle can lead to significant heat transfer enhancement when compared to applying uniform wall temperatures. However, this is achieved at the cost of increased entropy generation.

1. Introduction

Natural convective heat transfer in porous-media is extensively studied owing to its occurrence in various industrial and technological applications like packed-bed reactors [1–3], solar air heaters [4], greenhouses [5], energy storage [6], solid waste treatment [7] etc. In most of these applications, the temperature distribution at the walls is non-uniform. For example, in green houses and solar collectors, the angle at which the sun rays fall at the surface can result in non-uniform wall temperature. This can influence the convective flow and thus the effective heat transfer.

Several studies have been carried out to investigate the influence of non-uniform wall temperature on natural convection in fluid-only and porous-media filled cavities. Numerical simulations of bottom heated - top cooled fluid-only [8] and porous media-filled [9] cavities with non-uniform wall temperatures report an increase in heat transfer with increase in the magnitude of the non-uniformity of the wall temperature. Similarly, an enhancement in heat transfer occurs in a side-heated fluid-only filled-cavity with non-uniform wall temperature [10] along with a significant change in the flow pattern. Similar studies with porous media filled side-heated cavities also report changes in flow patterns and consequent change in Nusselt number with the change in amplitude [11,12] and wavelength of sinusoidal wall temperature variations [13,14]. The phase difference between the sinusoidal temperature variations at the hot and cold walls is observed to significantly affect the temperature distribution [15], especially at large wavelengths in the wall temperature variation. However, in contradiction to the above literature, a non-uniform heating of the bottom wall and cooling of the side walls in fluid-only [16] and porous-media filled-cavities [17] result in the lowering of overall heat transfer rate when compared to cavities with constant wall temperature.

To understand and quantify the loss and degradation of energy under various heating arrangements, various researchers have turned to use entropy generation [18] as a guiding pathway. Studies on entropy generation to optimize the heat transfer process in porous-media filled-cavities with different thermal boundary conditions [16,19], suggest that heating at discrete locations is an effective strategy for optimal thermal processing of materials. Studies on temperature distribution and heat transfer optimization in

* Corresponding author.
E-mail address: M.Chakkingal@tudelft.nl (M. Chakkingal).

https://doi.org/10.1016/j.ijheatmasstransfer.2019.119168

Nomenclature

k	Thermal conductivity, W/m K
ζ	Fraction of maximum non-dimensional temperature, $\theta_{\max}$
Ra_f	Rayleigh Number based on fluid properties, $\frac{g\beta_f \Delta T L^3}{\nu_f \alpha_f}$
Nu_f	Local Nusselt number based on fluid properties, $-\frac{L}{\Delta T}\left(\frac{\partial T}{\partial y}\right)_{wall}$
$< Nu_f >$	Area-weighted average of the local Nusselt number on the left and right walls.
θ	Non-dimensional temperature, $\frac{T-\overline{T_l}}{T_r-\overline{T_l}}$
θ_m	Non-dimensional volume-averaged temperature of fluid
T	Temperature, K
$\overline{T}$	Spatial mean temperature, K
ΔT	Mean temperature difference between the left and right walls $T_r-\overline{T_l}$, K
T_{ref}	Average temperature between the walls $\frac{T_r+\overline{T_l}}{2}$, K
c_p	Specific heat capacity, J/kg K
d	Diameter of sphere, m
$< >_{Vf}$	Averaged over volume of fluid
L	Height of cavity, m
$RMTD$	Root mean sq.deviation of temperature.
$\dot{S}_\theta$	Total volumetric non-dimensional entropy generation representation
f	Fluid
m	Volume-weighted average
s	Solid
l	Left wall
r	Right wall
θ_l^{amp}	Amplitude of non-dimensional sinusoidal wall temperature at the left wall
CWT	Constant wall temperature
$Vol(f)_{CD}$	Cumulative distribution of fraction of fluid volume
SWT	Sinusoidal wall temperature
Φ_{ph}	Phase angle of the non-dimensional sinusoidal wall temperature at the left wall
$\mathbf{u}$	Pore-scale velocity, m/s
$\mathbf{u}^*$	Non-dimensional pore-scale velocity, $\frac{\mathbf{u}}{U_0}$
Ψ	Irreversibility coefficient, $\frac{\nu\rho T_{ref}}{k}\left(\frac{\alpha}{L(T_r-\overline{T_l})}\right)^2$
U_0	Characteristic velocity scale, $\frac{Ra_f{}^{1/2}\alpha}{L}$, m/s
X, Y, Z	Represents the rectangular coordinate system
$\mathbf{g}$	Accel. due to gravity (acts along Z axis), m/s^2
p	Pressure, N/m^2
ρ	Density of fluid, kg/m^3
ν	Kinematic viscosity of fluid, m^2/s
ϕ	Porosity
β	Coefficient of volume expansion of fluid, K^{-1}
α	Thermal diffusivity,$(k/\rho c_p)$, m^2/s

fully and partially filled porous-media [20–22] indicate the strong influence of non-uniform temperature in entropy generation and pore-scale temperature distribution.

All the studies above on porous-media filled cavities are based on the Darcy assumption where one assumes that the porous length scales are small compared to flow and thermal scales, such that the detailed morphology of the porous medium does not influence the large scale flow and temperature distribution. However, in many real-life applications such as the ones reported above, the porous length scales are not small compared to their flow and thermal counterparts. Also, the variation in temperature distribution and the associated change in heat transfer demands for an in depth analysis of the influence of non-uniform temperature at the boundaries in systems where the flow and thermal scales are comparable to the pore-scale.

In our earlier work [23–25] we reported on the local flow and heat transfer in bottom-heated, top-cooled cavities with isothermal walls and filled with coarse grained porous media. In these studies we quantified the influence of material, packing, and size of coarse-grained porous-media on local flow and heat transfer at different Rayleigh number.

In the present work, we report detailed CFD simulations of a differentially heated coarse-grained porous-media filled-cavity with sinusoidal spatial variations in the wall temperature at different phase angles, to understand its influence on the local flow and temperature distribution and on entropy generation. We compare the flow and temperature distributions to those in a cavity with uniform wall temperatures. We also compare the results with water-only filled differentially heated cavities under similar conditions, to understand the influence of coarse-grained porous-media in enhancing/suppressing heat transfer.

2. Mathematical formulations and numerical methods

2.1. Physical problem

We analyze natural convection in a porous-media filled $L \times L \times L$ cubical cavity, with side-heated and side-cooled vertical walls. Water is used as the fluid ($Pr_f = 5.4$). The coarse-grained porous-media is composed of relatively large spherical hydrogel beads arranged in structured Simple Cubic Packing (SCP), resulting in a porosity, $\phi = 0.48$. A Simple Cubic Packing has pores that are geometrically similar to connected vertical and horizontal channels, facilitating flow channelling even at lower Rayleigh numbers and thus increasing the impact of the morphology of the coarse-grained packing on the thermal and flow behaviour. We choose the ratio of the diameter of the beads, d to the length of the cavity, L to be 0.2. The use of hydrogel beads results in a solid-to-fluid thermal conductivity ratio $k_s/k_f = 1$. The flow in differentially heated cavities at the Rayleigh numbers discussed later, is steady and laminar in nature. We numerically solve the steady-state incompressible Navier-Stokes equations and the energy equation for the fluid, and the energy equation for the solid. The heat transfer between the solid and the fluid domain results in a conjugate heat transfer problem. With the Boussinesq approximation ($\beta\Delta T << 1$)[26], all fluid properties are taken to be constant, except for the fluid density in the body-force term included in the Navier–Stokes equations.

Fluid phase:

$$\nabla \cdot \mathbf{u} = 0 \tag{1}$$

$$\mathbf{u} \cdot \nabla \mathbf{u} = -\frac{1}{\rho}\nabla p + \nu \nabla^2 \mathbf{u} + \mathbf{g}\beta(T_f - T_{ref}) \tag{2}$$

$$\mathbf{u} \cdot \nabla T_f = \alpha_f \nabla^2 T_f \tag{3}$$

Solid phase:

$$\alpha_s \nabla^2 T_s = 0 \tag{4}$$

For used symbols, refer to the List of Nomenclature.

2.2. Numerical method

For our porous media filled cavity simulations the above set of equations, Eqs. (1)–(4) is discretized and steady-state numerical simulations [27] are carried using the conjugate heat transfer solver, "conjugateHeatSimpleFoam" available in foam-extend-4.0 [27], a fork of the OpenFOAM open source library for Computational Fluid Dynamics. We use unstructured tetrahedral grids to simulate the packed bed cavities. The capability of OpenFOAM to simulate flow using arbitrary tetrahedral meshes is discussed in [28–30]. Details of our solver validation are discussed in Appendix A. The fluid temperature Eq. (3) and the solid temperature Eq. (4) of the conjugate heat transfer problem are combined into a combined matrix equation, by the method of block coupling [31,32]. Thus the fluid flow equation is solved in the fluid region only, and the energy equation, discretised separately on the fluid and solid regions, is solved in a single linear solver call. This ensures a strong coupling between the solid and fluid regions. For water-only filled cavities we solve Eqs. (1)–(3) using the OpenFOAM solver "BuoyantBoussinesqSimpleFoam", which is validated against the results reported in [33]. Here we use structured grids.

For both water-only and porous-media filled-cavities, a 2nd order central differencing scheme, defined as "limitedLinear1" in OpenFOAM, is used for the convective and diffusive terms [27]. The pressure-velocity-coupling at each iteration is handled by the iterative SIMPLE algorithm [34]. The energy transport equation Eq. (3), is solved with the divergence-free velocity obtained in each iteration.

2.3. Geometry and boundary conditions

The simulations are carried out at Ra_f varying from 10^5 to 10^7. To analyze the data, the temperature and velocity are expressed in non-dimensionalized form (refer Nomenclature). The right wall of the cavities is maintained at a constant non-dimensional temperature, $\theta_r = 1$. The left wall of the cavity is maintained at:

1. a constant temperature (CWT), $\theta_l = 0$, or
2. a sinusoidally varying wall temperature (SWT):

$$\theta_l(z) = \theta_l^{amp} \sin\left(\frac{2\pi z}{L} + \Phi_{ph}\right) \tag{5}$$

with a mean temperature, $\overline{\theta_l} = 0$. The phase angle Φ_{ph} varies from -180° to 180° (see Fig. 1).

The influence of the amplitude of the sinusoidal temperature variation is studied by using two non-dimensional amplitudes, $\theta_l^{amp} = 0.5$ and 1. The phase angle, Φ_{ph} of the sinusoidal wall temperature variation is also varied. The system with CWT can also be visualized as a system with SWT, where $\theta_l^{amp} = 0$. All the other vertical and horizontal walls of the cavity are adiabatic. No-slip boundary condition is applied at all solid surfaces. Grid independence studies are carried out using three different unstructured tetrahedral grids with 1.9×10^6 (uniform grid size, $\Delta \approx d/16$), 5×10^6 (non-uniform grid size, $\Delta \approx d/16$ in the core and $\Delta \approx d/32$ at the walls of the cavity) and 1.03×10^7 cells (non-uniform grid size, $\Delta \approx d/16$ in the core and $\Delta \approx d/64$ at the walls of the cavity), at $Ra_f = 10^7$. Comparing the two finest meshes, a deviation in $< Nu_f >$ of ~ 1% is observed for the case with maximum $< Nu_f >$ and a difference of ~ 0.8% in the case with minimum $< Nu_f >$. Therefore, the simulations at $Ra_f = 10^6$ and $Ra_f = 10^7$ are carried out with 5×10^6 and 1.9×10^7 cells respectively. We also confirm the quality of the mesh by comparing the degree of uniformity of temperature distribution $RMTD_m$ (as defined later in Eq. (8)) in the porous-media-filled cavity with the highest Nusselt number ($Ra_f = 10^7, \theta_l^{amp} = 1,\ \Phi_{ph} = -45^\circ$) in which $RMTD_m$ changes by 2.2% when the mesh is refined from 5×10^6 to 1.9×10^7 cells. For the water-only filled cavity simulations, a grid independence study is carried out using 3 different structured grids; 32^3, 64^3 and 128^3 with a grid expansion ratio of 1.2. The deviation in maximum Nusselt number and $RMTD_m$ obtained with 64^3 and 128^3 are ~ 0.15% and ~ 0.5% respectively. Thus, the water-only filled-cavity simulations are carried out with the finest grid, 128^3.

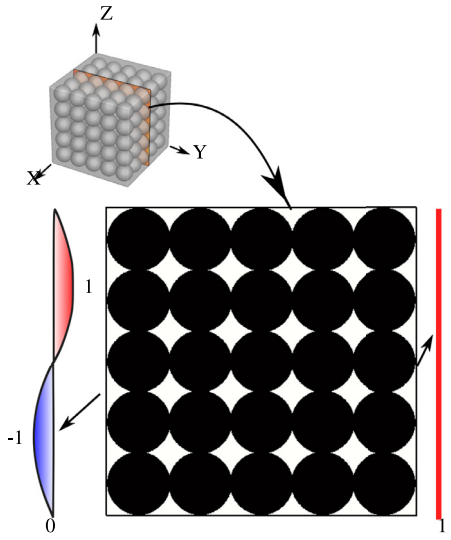

Fig. 1. Geometrical representation of the differentially heated water filled cavity with hydrogel beads. The left wall has a sinusoidal non-dimensional temperature, with mean value $\overline{\theta_l} = 0$ and amplitude $\theta_l^{amp} = 1$; and the right wall is maintained at a constant non-dimensional temperature $\theta_r = 1$.

3. Results and discussion

The heat transfer, flow and temperature distributions in the porous-media filled-cavities are compared to the results from water-only filled-cavities with CWT and SWT arrangements at various phase angles Φ_{ph}, three different $Ra_f = (10^5, 10^6, 10^7)$ and temperature variation amplitudes θ_l^{amp} ={0.5, 1}.

3.1. Wall averaged heat transfer

To understand the influence of a sinusoidal wall temperature variation and its phase angle at different Ra_f, we focus on the wall averaged Nusselt numbers, $< Nu_f >$ (Fig. 2). The wall-averaged Nusselt number is defined as the area-weighted value of the local Nusselt Number on the left and right walls.

The Nusselt numbers in water-only and porous-media filled cavities with SWT at $\theta_l^{amp} = 1$ and different phase angles, are compared with the cavities at CWT. For both CWT and SWT, the Nusselt number in water-only filled-cavity (Fig. 2(a)) and porous-media filled-cavity (Fig. 2(b)) increases with an increase in Ra_f. The wall-averaged Nusselt numbers obtained for water-only filled cavities with CWT follow the correlations [33]:

$$< Nu_f >= \begin{cases} 0.136 \times {Ra_f}^{0.305} & 700 < Ra_f \le 10^6 \\ 0.236 \times {Ra_f}^{0.265} & 10^6 > Ra_f \end{cases}$$

with less than 2% deviation. Lower heat transfer is found in porous media filled CWT cavities.

With SWT non-uniform wall temperatures, the Nusselt number not only depends on Ra_f, but also on the amplitude θ_l^{amp} and the phase change Φ_{ph} of the sinusoidal temperature variations. In water-only filled cavities (Figs. 2(a) and 3), an amplitude $\theta_l^{amp} = 1$ leads to a maximum heat transfer enhancement

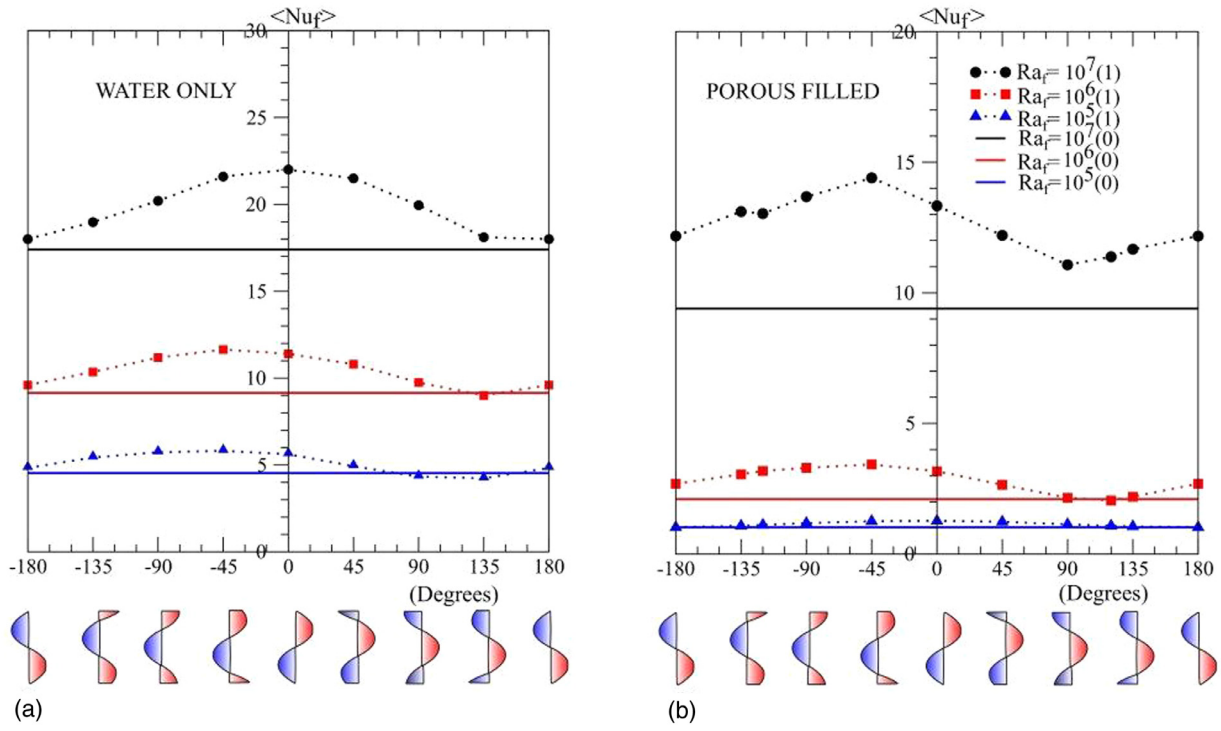

Fig. 2. Variation of wall-averaged Nusselt number with phase angle at different Rayleigh numbers ($Ra_f = 10^5, 10^6, 10^7$) and different amplitudes, $\theta_l^{amp} = 0$(CWT), 1 in water-only (a) and porous media filled (b) cavity.

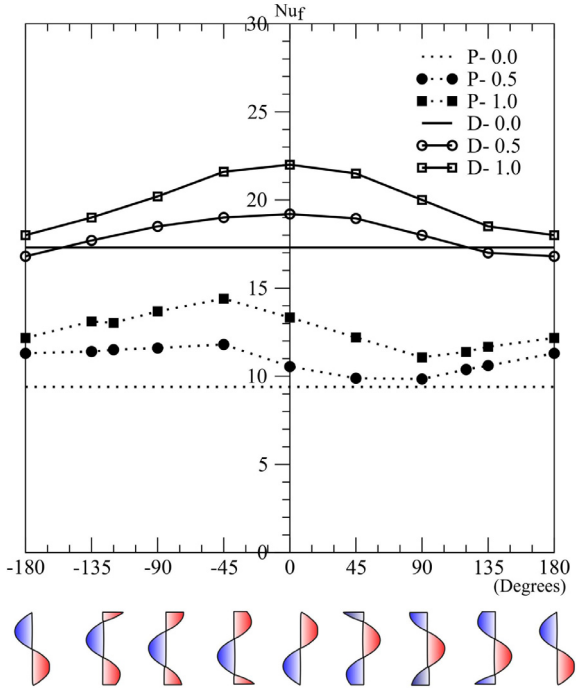

Fig. 3. Variation of wall-averaged Nusselt number with phase angle at $Ra_f = 10^7$ and different amplitudes, θ_l^{amp} (0, 0.5, 1) of cold wall temperature variation in a differentially heated water-only cavity (**D**) and porous media filled-cavity (**P**).

of approximately 30% at $\Phi_{ph} = -45^\circ$ for $Ra_f = 10^5 - 10^6$, and at $\Phi_{ph} = 0^\circ$ for $Ra_f = 10^7$. This maximum heat transfer enhancement decreases with decreasing θ_l^{amp} (Fig. 3). At some values of the phase changes Φ_{ph}, the application of varying wall temperatures may lead to a decrease in heat transfer, for instance at $Ra_f = 10^7$,

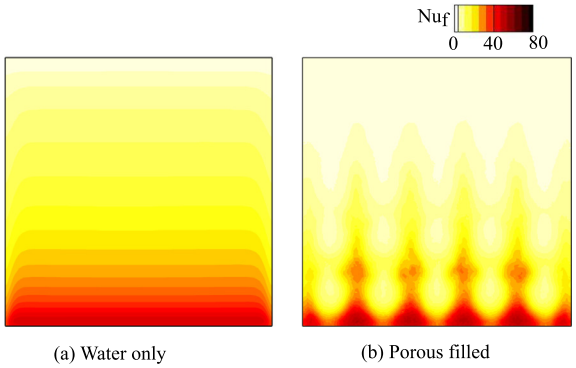

Fig. 4. Nusselt number contour on the right wall in a water-only (a) and porous media filled (b) cavity, with constant temperature of $\theta_l = 0$ and $\theta_r = 1$, at $Ra_f = 10^7$. The contours are represented using a linear scale with 30 contour levels.

$\theta_l^{amp} = 0.5$ and $\Phi_{ph} = 180^\circ$ (Fig. 3). In porous medium filled cavities, (Figs. 2(b) and 3), an amplitude $\theta_l^{amp} = 1$ leads to a maximum heat transfer enhancement of approximately 60% at $\Phi_{ph} = -45^\circ$ for $Ra_f = 10^5 - 10^7$. Again, this maximum heat transfer enhancement decreases with decreasing θ_l^{amp} (Fig. 3). A decrease in heat transfer due to the application of non-uniform wall temperatures is not observed for porous medium filled cavities.

3.2. Local Nusselt number distribution

At first, we analyze the local Nu_f distribution at the right wall of both fluid-only and porous-media filled cavities (Fig. 4) with CWT. The maximum heat transfer in a water-only cavity (Fig. 4(a)) is uniformly distributed along the horizontal direction at the bottom of the right wall. In a porous-media filled cavity (Fig. 4(b)) the maximum heat transfer is limited to the pore-space close to the

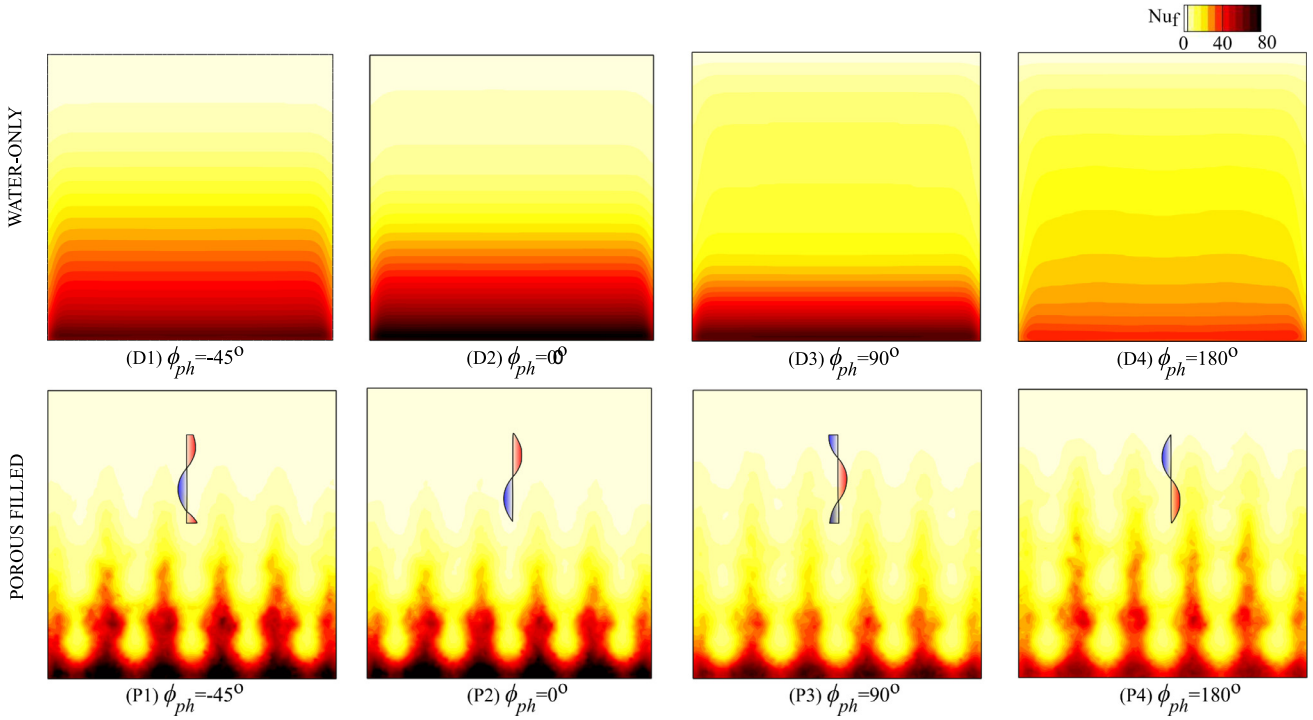

Fig. 5. Nusselt number contour at the right wall in a water-only (**top row**) and porous media filled (**bottom row**) cavity, with the left wall having sinusoidal temperature distribution of amplitude $\theta_l^{amp} = 1$ and varying phase angle Φ_{ph}, at $Ra_f = 10^7$. The contours are represented using a linear scale with 30 contour levels.

bottom of the right wall resulting in a non-uniform heat transfer along the horizontal direction.

The heat transfer at the right wall in the porous-filled cavity is very low over a large fraction of the wall area, with heat transfer at the top being close to that due to pure conduction. The hydrogel beads obstructing the flow result in lower flow velocities in the porous-filled cavity (Fig. 6(b)) when compared to the fluid-only cavity (Fig. 6(a)). The obstructed flow at the top of the porous-filled cavity results in a conduction dominated temperature distribution near the top of the right wall, unlike the water-only filled cavity in which the temperature distribution is governed by convection.

To understand the influence of varying temperature distribution, a sinusoidal wall temperature with $\theta_l^{amp} = 1$ and different phase angle, Φ_{ph} is applied at the left wall. We analyze its influence on the Nu_f distribution at the right wall (which has a constant wall temperature $\theta_r = 1$) of water-only filled cavities and porous-media filled cavities in Fig. 5.

In both the cavities, the Nusselt number distribution at the right wall is influenced by the phase angle of the sinusoidal left wall temperature. In water-only cavities (Fig. 5(D1–D4)), the maximum increase in heat transfer is observed at $\Phi_{ph} = 0^\circ$ (D2) while a maximum heat transfer in porous-media filled cavities is observed at $\Phi_{ph} = -45^\circ$ (Fig. 5(P1)). Similar to the porous-media filled cavities with CWT (Fig. 4), the Nusselt number distribution at the top of the right wall in porous-media filled cavities with SWT (Fig. 7(P1–P4)) is low owing to the hydrogel beads obstructing the flow, which again results in a conduction dominated temperature distribution near the top of the right wall.

3.3. Local thermal and flow features

The difference in local heat transfer between CWT and SWT, and its dependence on the phase angle in the latter, hints at variations in local temperature and flow features, which are further discussed in this section. The flow velocities **u** are non-dimensionalized with a characteristic velocity scale, U_0 (refer nomenclature) [35], such that:

$$\mathbf{u}^* = \frac{\mathbf{u}}{U_0} \tag{6}$$

Similarly, the temperature is non-dimensionalized with the right wall and average left wall temperature (refer nomenclature). In Fig. 6 we analyze the flow and temperature distribution at $Ra_f = 10^7$, in a characteristic vertical plane at $X/L = 0.41$, in a water-only and porous medium filled-cavity at CWT. In the water-only cavity, large flow velocities are found in the thin boundary layers adjacent to the vertical walls. In the porous media filled cavity, the flow velocity is low resulting in comparatively thicker thermal boundary layers.

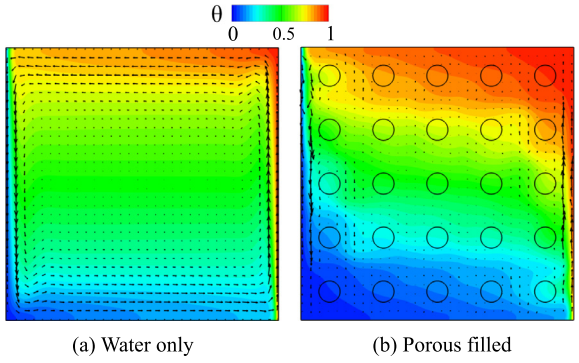

Fig. 6. Non-dimensional temperature contours and velocity vectors in a vertical plane at $X/L = 0.41$ in a water-only (a) and porous media filled (b) cavity, with constant temperature $\theta_l = 0$ and $\theta_r = 1$, at $Ra_f = 10^7$. The contours are represented using a linear scale with 30 contour levels.

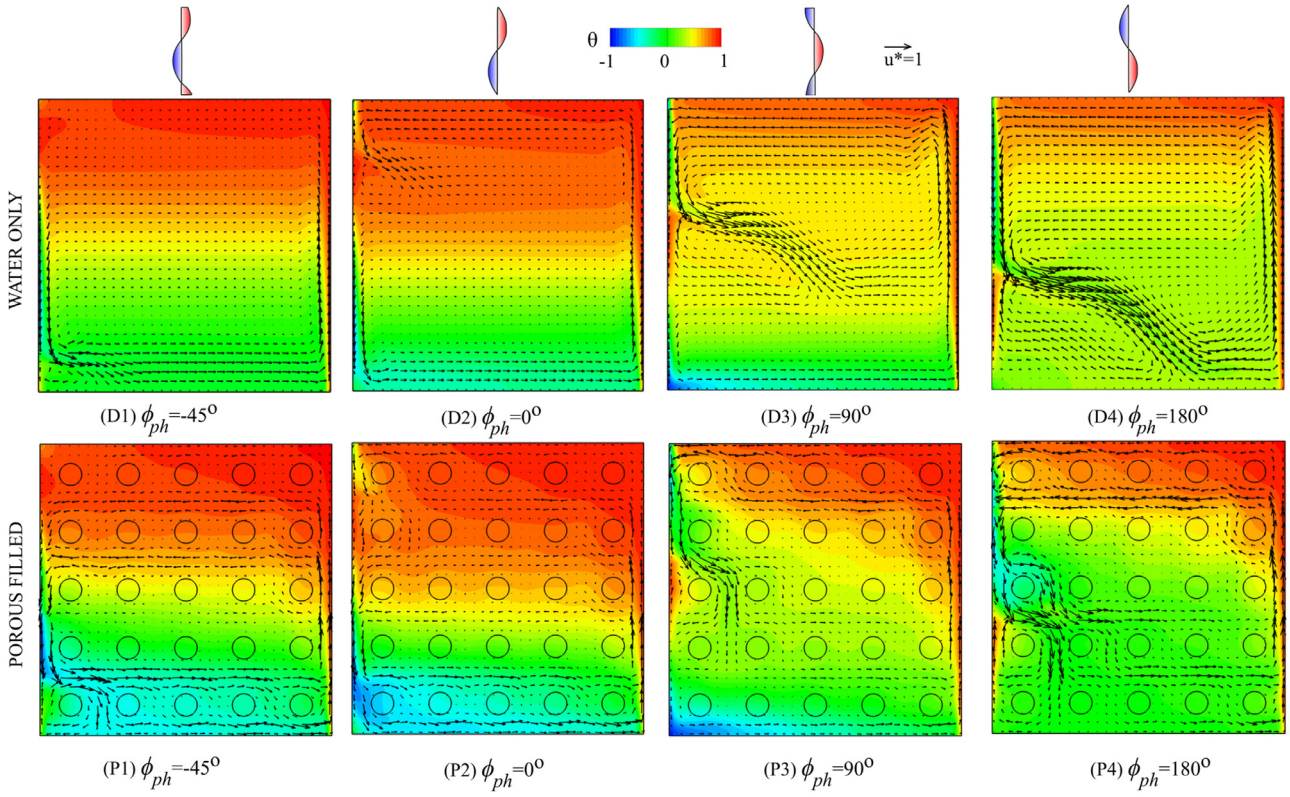

Fig. 7. Non-dimensional temperature contours and velocity vectors in a vertical plane at $X/L = 0.41$ in a water-only (**top row**) and porous media filled (**bottom row**) cavities, with the left wall having a sinusoidal temperature distribution with amplitude $\theta_l^{amp} = 1$ and varying phase angle Φ_{ph}, at $Ra_f = 10^7$. The contours are represented using a linear scale with 30 contour levels.

When a sinusoidal temperature distribution at different phase angles is applied at the left wall, the flow and temperature distributions change considerably (Fig. 7) varying from stable temperature stratification with virtually no flow at the top of the cavity for $\Phi_{ph} = -45^\circ$ (Fig. 7 (D1 and P1)) to flow penetrating into the core of the cavities at $\Phi_{ph} = 90^\circ$ and 180° (Fig. 7(D3 and D4, P3 and P4)). In the water-only cavity (Fig. 7(D3 and D4)), a large difference in the flow along the left and right wall is observed. However, no significant enhancement in heat transfer is obtained owing to the fluid impinging the right wall at a higher temperature (when compared to Fig. 6(a)). In a porous media filled cavity (Fig. 7(P1)), the colder fluid moving down the left wall is deviated to the right wall by the porous media, resulting in fluid at lower temperature to impinge the right wall and thus leading to an enhanced heat transfer when compared to the cavity at CWT, as observed in Fig. 2(b). However, the heat transfer is lower than in a fluid-only cavity with similar wall temperature distribution (Fig. 2(b)) owing to a lower flow velocity. The current observation indicates that the combined effect of variations in local porosity close to the wall and the local wall temperature can result in strong local and overall variations in heat transfer.

As discussed earlier, the integral heat transfer varies with the wall temperature distribution in both the water-only (Fig. 2(a)) and porous media (Fig. 2(b)) filled cavities. To understand this behaviour, we look at the local pore-scale temperature and horizontal flow velocity in both water-only and porous-media filled cavities close to the right wall, at $Ra_f = 10^7$. We already see from the Nusselt number contours that the maximum heat transfer from the right wall occurs at the bottom, and varies with the local temperature distribution at the left wall. The local pore-scale temperature along the vertical line $Y/L = 0.8$ in the plane $X/L = 0.41$ in both water-only (Fig. 8(a)) and porous media filled (Fig. 8(b)) cavties,

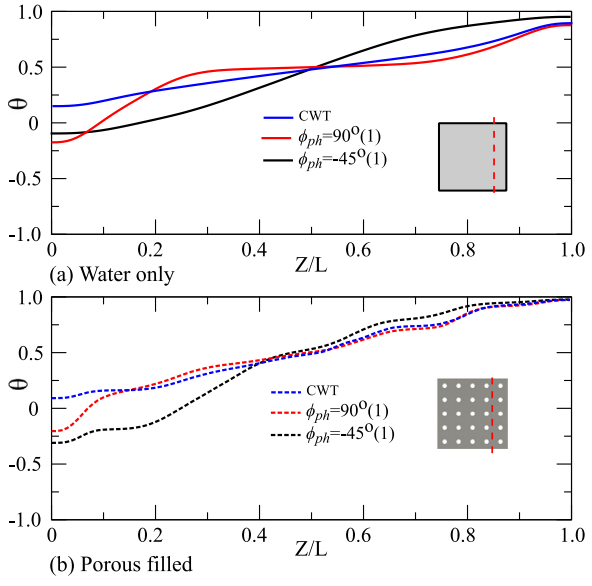

Fig. 8. Non-dimensional temperature along the vertical line $Y/L = 0.8$, in a vertical plane at $X/L = 0.41$ in water-only (a) and porous media filled (b) cavities, with the left wall having a sinusoidal temperature distribution with amplitude $\theta_l^{amp} = 1$ at $\phi_{ph} = 90^\circ$ (red) and -45° (black), at $Ra_f = 10^7$. The results are compared with the respective cavities at constant wall temperature (blue). (For interpretation of the references to color in this figure legend, the reader is referred to the web version of this article.)

close to the bottom of the right wall also varies strongly with the change in ϕ_{ph} of the SWT distribution. In the water-only filled cavities, the temperature at the bottom is lower in cavities with

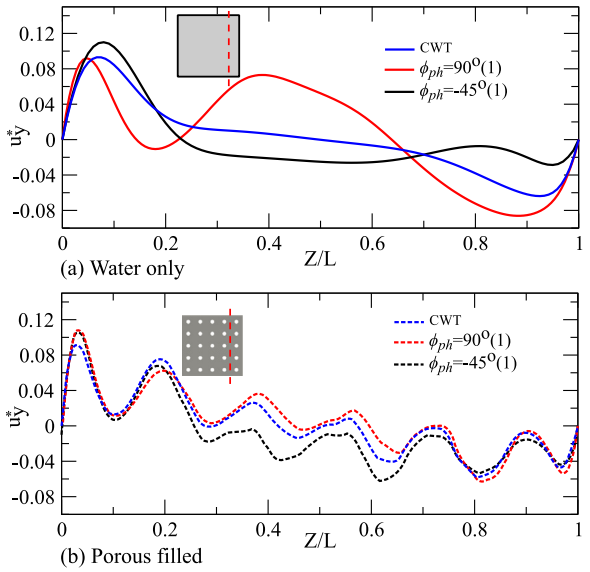

Fig. 9. Non-dimensional horizontal velocity (u_y^*) along the vertical line $Y/L = 0.8$, in a vertical plane at $X/L = 0.41$ in water-only (a) and porous media filled (b) cavities, with the left wall having a sinusoidal temperature distribution with amplitude $\theta_l^{amp} = 1$ at $\phi_{ph} = 90^\circ$ (red) and -45° (black), at $Ra_f = 10^7$. The results are compared with the respective cavities at constant wall temperature (blue). (For interpretation of the references to color in this figure legend, the reader is referred to the web version of this article.)

SWT than in the cavity with CWT (Fig. 8(a)). The non-dimensional horizontal velocity u_y^*, with which the fluid impinges on the right wall, is higher in the cavity with SWT at $\phi_{ph} = -45^\circ$ (Fig. 9(a)), resulting in higher heat transfer (among the cases considered in the line plot) followed by the cavities with SWT at $\phi_{ph} = 90^\circ$ and CWT. While in the porous media filled cavities, the combination of lower fluid temperature (Fig. 8(b)) and higher non-dimensional horizontal velocity u_y^* (Fig. 9(b)) (with which the fluid impinges on the right wall) is observed in the cavity with SWT at $\phi_{ph} = -45^\circ$ followed by the cavities with SWT at $\phi_{ph} = 90^\circ$ and CWT. Thus the combined effect of local temperature and velocity of the fluid results in the variation in heat transfer in both water-only and porous media filled cavities. Since the influence of the packing varies with the location of the plane, the effect of the variation in the local wall temperature of the left wall can be better understood from the domain averaged features.

3.4. Domain averaged thermal and flow features

To understand the reason for the variation in heat transfer with amplitude and phase angle of SWT in the water-only and porous-media-filled cavity, we focus on volume-averaged temperature as discussed in the literature [36,37]. The volume-averaged temperature of the fluid region θ_m defined as:

$$\theta_m = \frac{\int\int\int \theta_f d\Omega_f}{\int\int\int d\Omega_f} \tag{7}$$

varies in water-only and porous media filled cavities with Ra_f (Fig. 10). In water-only filled-cavities and porous media-filled cavities at constant wall temperature $\theta_m = 0.5$ (Fig. 10(D1 and P1)) for all Ra_f. However, with a sinusoidal wall temperature, a variation in θ_m occurs with the change in phase angle and Rayleigh number, with a strong variation in porous-media filled cavities (Fig. 10(P1)). The degree of uniformity of temperature distribution in the cavities is quantified by calculating $< RMTD >_m$ defined as:

$$RMTD_m = \sqrt{\frac{\int\int\int (\theta_f - \theta_m)^2 d\Omega_f}{\int\int\int d\Omega_f}} \tag{8}$$

The value of $RMTD_m$ ranges between 0 and 1, with a low of $RMTD_m$ indicating higher degree of uniformity in the fluid temperature.

In a water-only filled-cavity with constant wall temperature ($\theta_l^{amp} = 0$), the $RMTD_m$ (Fig. 10(D2)) decreases with an increase in Ra_f. When a sinusoidal wall temperature is applied at the left wall, a variation in the $RMTD_m$ with phase angle Φ_{ph}, is observed. We observe the highest degree of temperature non-uniformity at $\Phi_{ph} = 0^\circ$, and the smallest at $\Phi_{ph} = 180^\circ$. The minimum is less than the value in the cavity with constant wall temperature, indicating an increase in temperature uniformity with SWT at $\Phi_{ph} = 180^\circ$ over the uniformity with constant wall temperature.

Unlike in a water-only cavity, in a porous-media filled-cavity with constant wall temperature, we observe a decrease in thermal uniformity with an increase in Ra_f. The increased flow close to the wall of the cavity results in a higher temperature difference between the regions close to the wall and core of the porous-media filled-cavity, eventually resulting in the increase in thermal non-uniformity with an increase in Ra_f. Strong variation in thermal uniformity with phase angle and Rayleigh number is visible in porous media filled cavities (Fig. 10(P2)). The $RMTD_m$ in porous-media filled cavities at different phase angles and Rayleigh numbers are always higher than in a cavity with constant wall temperature.

The $RMTD_m$ gives an indication of uniformity in the cavities, but still doesn't completely explain the trend we observe in the Nusselt number (Fig. 2). We can better understand the trend from the cumulative distribution of the fluid-volume of the cavity with the non-dimensional temperature ranging between $\theta_r = 1$ and $\overline{\theta_l} = 0$ (Fig. 11) at a SWT amplitude of 1 and $Ra_f = 10^7$. In water-only cavities (Fig. 11(a)) the fraction of fluid volume at temperatures close to 1 (right wall temperature) is higher at $\phi_{ph} = 0^\circ$ and -45° and so is the fluid at temperatures below 0 (mean left wall temperature). While in the cavity with SWT at $\phi_{ph} = 180^\circ$ and in the cavity with CWT, the fraction of fluid-volume with temperature close to 1 is comparatively lower and no fraction of fluid volume has a temperature below 0. We obtain higher heat transfer in cavities with higher fraction of volume at temperature close to 1 and below 0 ($\phi_{ph} = 0^\circ$ and -45°), and heat transfer comparable to cavity at constant wall temperature in the cavity with SWT at $\phi_{ph} = 180^\circ$. Similar behaviour is observed in porous media filled cavities (Fig. 11(b)). However, the heat transfer in the cavity at $\phi_{ph} = 180^\circ$ is greater than in the cavity with CWT (Fig. 2(b)), due to the increased fraction of fluid at temperature lower than 0.

The increased values in $RMTD_m$ indicate the presence of strong temperature gradients which can result in the production of thermal entropy and thus increased thermodynamic irreversibility. In the current study the irreversibility coefficient Ψ, the ratio between the viscous and thermal irreversibilities [18] defined as:

$$\Psi = \frac{\nu \rho T_{ref}}{k} \left(\frac{\alpha}{L(T_r - \overline{T_l})} \right)^2 \tag{9}$$

is $< < 1$. Thus, unlike cases where the contribution by the viscous dissipation is significant (as for example [38,39]) the contribution of viscous dissipation to the total entropy generation is very low and is thus neglected in our analysis.

The local thermal entropy generated in the fluid, $\dot{S}_T'''$ is calculated as:

$$\dot{S}_T''' = \frac{k_f}{T_f^2} \nabla T_f \cdot \nabla T_f \tag{10}$$

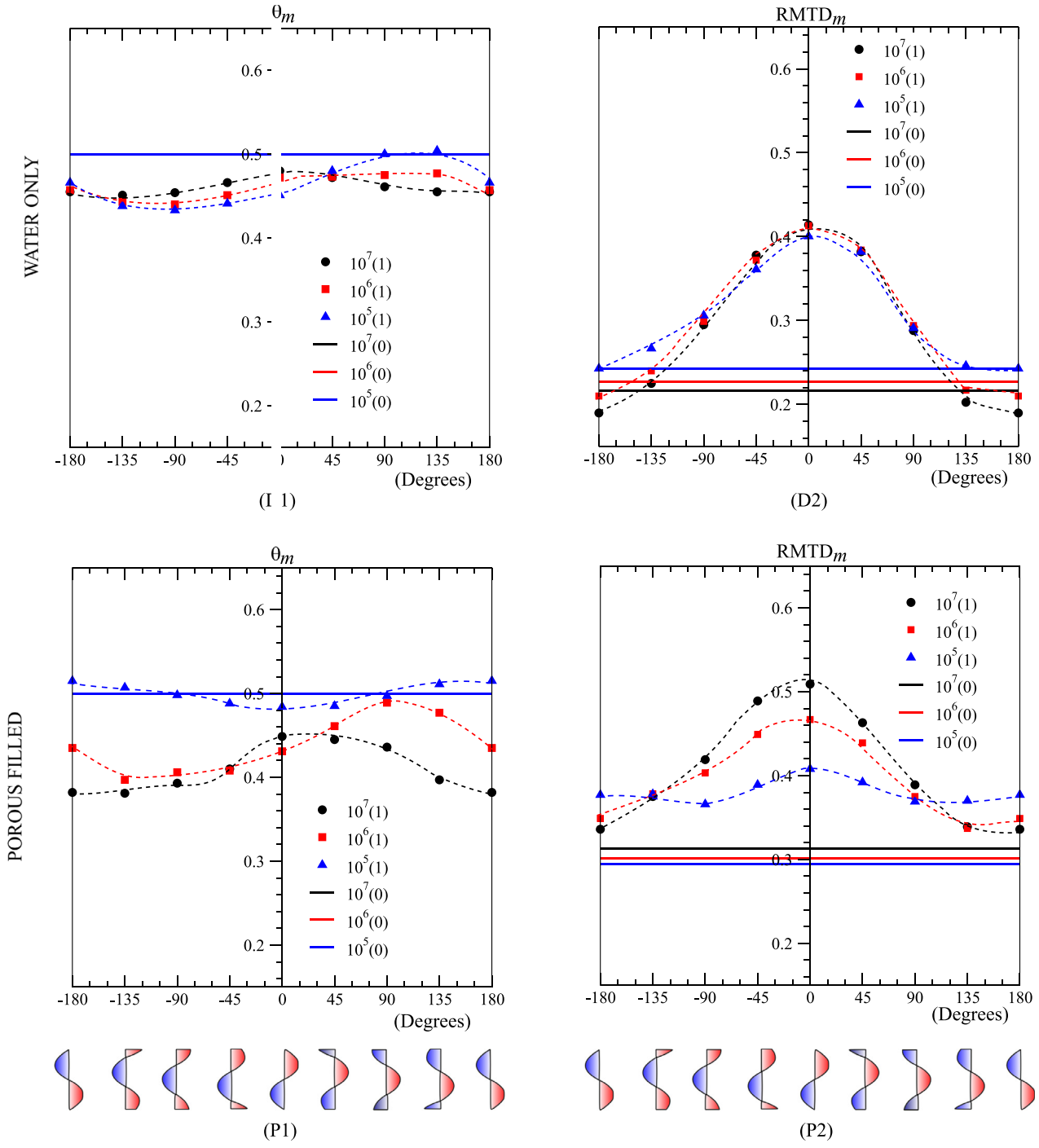

Fig. 10. Variation of non-dimensional volume-averaged mean temperature (**D1, P1**) and $RMTD_m$ (**D2, P2**) of the fluid, with phase angle at different Rayleigh numbers ($Ra_f - 10^5, 10^6, 10^7$) and different amplitudes (0, 1) of sinusoidal wall temperature in a water-only (**top row**) and porous media filled (**bottom row**) cavity. The dotted lines are only to guide the eyes.

It is scaled as:

$$\dot{S}_\theta''' = \frac{\dot{S}_T'''}{\frac{k_f}{T_{ref}^2}\left(\frac{\Delta T}{L}\right)^2} \tag{11}$$

for our visualizations reported in Figs. 12 and 13.

To compare the total entropy generated in the fluid region for different thermal configurations, we also define the total thermal entropy generated in the cavities as:

$$\dot{S}_T = \int\int\int \dot{S}_T''' d\Omega_f \tag{12}$$

where, the integration is carried out over the fluid volume only.

It is scaled as:

$$\dot{S}_\theta = \frac{\dot{S}_T}{\frac{k_f}{T_{ref}^2}\left(\frac{\Delta T}{L}\right)^2 L^3} \tag{13}$$

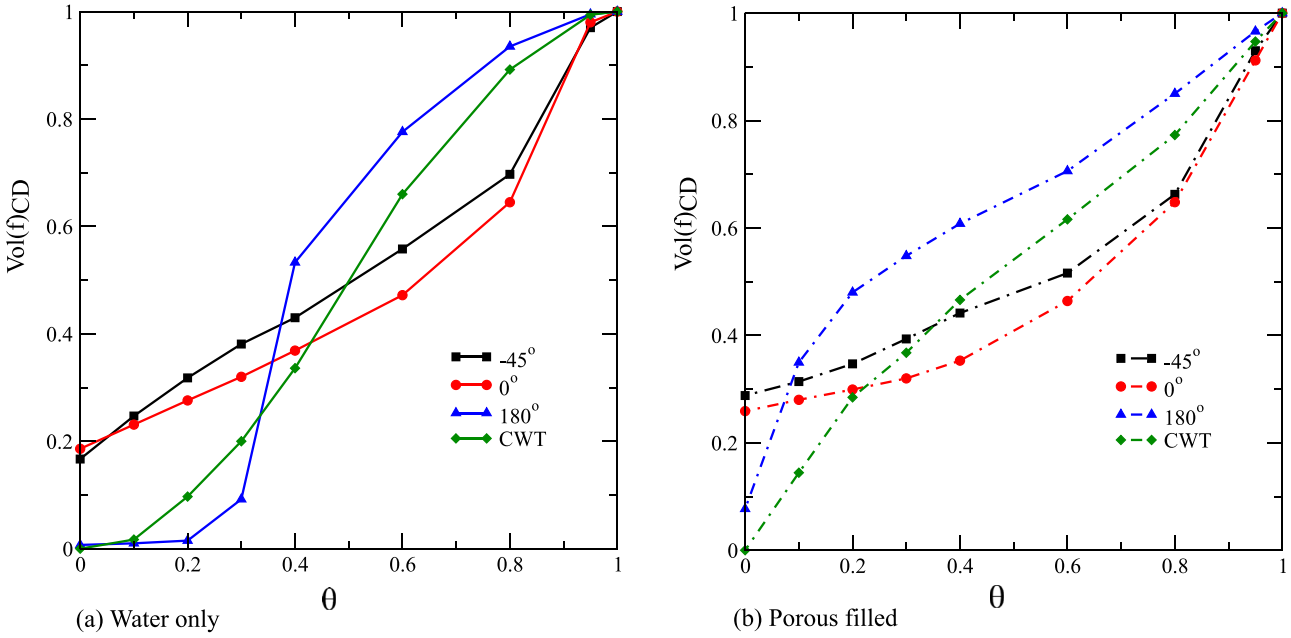

Fig. 11. Cumulative distribution (discrete) of the fraction of fluid volume where $\theta \leq \zeta\theta_{\max}$, in water-only (a) and porous media filled (b) cavities, with the left wall having a sinusoidal temperature distribution with amplitude $\theta_l^{amp} = 1$ at $\phi_{ph} = -45^\circ$ (black), $\phi_{ph} = 0^\circ$ (red), $\phi_{ph} = 180^\circ$ (blue) at $Ra_f = 10^7$. The results are compared with the respective cavities at constant wall temperature (green). (For interpretation of the references to color in this figure legend, the reader is referred to the web version of this article.)

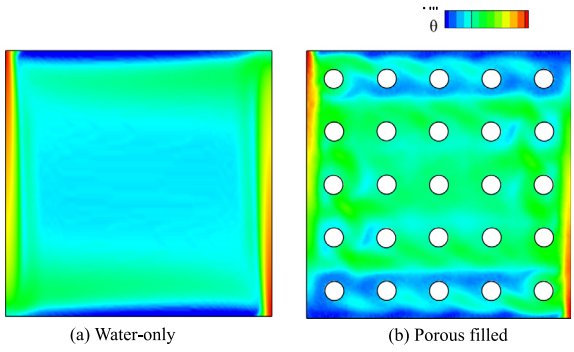

Fig. 12. Entropy generated due to temperature gradient in the fluid region (log scale) in a characteristic vertical plane at $X/L = 0.41$ in a water-only (a) and porous media filled (b) cavity, with constant temperature left wall $\theta_l = 0$ and right wall temperature $\theta_r = 1$, at $Ra_f = 10^7$.

for the comparison of the different configurations reported in Fig. 14.

In Fig. 12(a and b), we observe that the non-dimensional thermal entropy generated in both fluid-only and porous medium filled cavities is higher close to the bottom and top of the vertical walls, where the temperature gradient is higher. The presence of spherical beads results in a comparatively higher temperature gradient at the core of the cavity (Fig. 12(b)) than in a water-only cavity (Fig. 12(a)), resulting in higher entropy generation. However, the flow of fluid "close to saturated temperature" (Fig. 6(b)), redirected by the porous beads, results in lower temperature gradients at the pore-space close to the horizontal walls resulting in lower entropy generation (Fig. 12(b)).

As expected, the influence of SWT on the local temperature distribution results in a change in entropy generated in both the cavities. The entropy generation in cavities with sinusoidal wall temperature variation (Fig. 13(D1–D4, P1–P4)) is higher than in cavities with constant wall temperature (Fig. 12(a and b)). In a water-only filled-cavity with SWT at $\Phi_{ph} = -45^\circ$, a decrease in the temperature gradient (Fig. 7(D1)) close to the bottom and top of the cavity results in a lower entropy generation at these locations than in the cavity with constant wall temperature. However, the temperature gradient close to the vertical walls and in the core of the cavity increases, resulting in higher entropy generation at these locations than in the case with constant wall temperature. A shift in the regions with a lower entropy generation is evident from Fig. 13(D1–D4). Close to the left wall of the water-only filled-cavity, we observe streaks of higher entropy generation which increase in size with increasing phase angle. With the change in phase angle, Φ_{ph} the locations at which maximum entropy is generated also changes. The presence of porous-media also results in an increase in entropy generation at all the phase angles (Fig. 13(P1–P4)), when compared to the water-only cavities. The long streaks of entropy generation observed in the water-only cavities close to the left wall vanishes in the porous-media filled cavities. The spherical beads suppress and redirect the flow (Fig. 7(P1–P4)), resulting in shorter/no streaks with high values of entropy generation. Instead of longer streaks of high entropy generation in the water-only cavity, the presence of spherical beads results in an increased entropy generation in the core of the cavity.

In Fig. 14 we compare the average volumetric entropy generation (averaged over fluid volume) at $Ra_f = 10^7$, with constant wall temperature and sinusoidal wall temperature at different phase angles. The average volumetric entropy generation, $< \dot{S}_\theta >_{Vf}$ in all the thermal configurations is scaled with the average volumetric entropy generated in a water-only filled-cavity with constant wall temperature, $< \dot{S}_{\theta D(0)} >_{Vf}$. From Fig. 14, we observe that the total volumetric entropy generation in a water-only filled-cavity with sinusoidal wall temperature is roughly a factor 2 higher than in the water-only filled-cavity with constant wall temperature. The influence of the phase angle results in the maximum entropy gener-

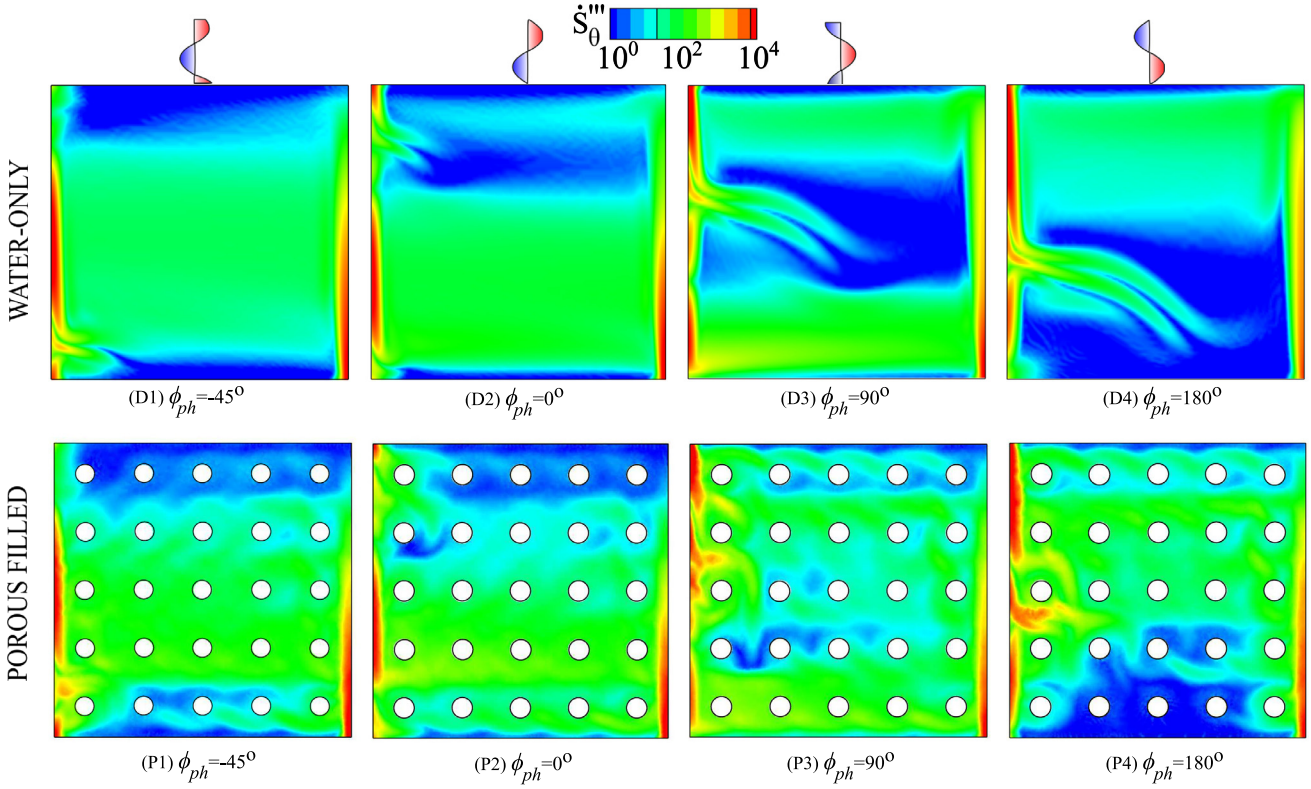

Fig. 13. Entropy generated in the fluid region due to temperature gradient in a characteristic vertical plane at $X/L = 0.41$ in a water-only (**top row**) and porous media filled (**bottom row**) cavity, with the left wall having sinusoidal temperature distribution with amplitude $\theta_l^{amp} = 1$ and varying phase angle Φ_{ph}, at $Ra_f = 10^7$.

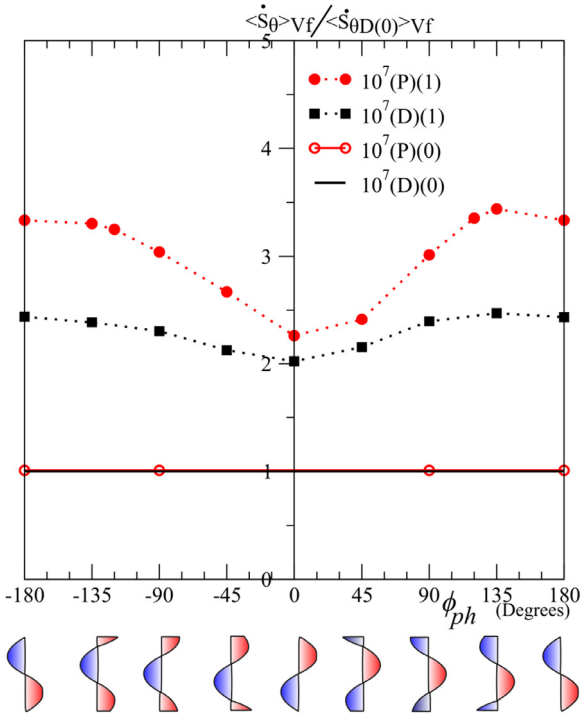

Fig. 14. Variation of non-dimensional entropy generation of fluid due to temperature gradient with phase angle at $Ra_f = 10^7$, with SWT ($\theta_l^{amp} = 1$) and CWT ($\theta_l^{amp} = 0$) in a water-only **(D)** and porous media filled **(P)** cavity.

ation at $\Phi_{ph} \approx \pm 135^\circ$ and a minimum entropy generation at $\Phi_{ph} \approx 0^\circ$. In a porous-media filled-cavity we see a similar effect of non-uniform wall temperatures on entropy production, but with an even larger increase.

4. Summary and conclusion

We studied the influence that applying a spatially varying wall temperature to one of the thermally active vertical walls has on the flow and heat transfer in a differentially heated, water-filled, cubical cavity packed with relatively large spherical hydrogel beads. We showed that the phase angle and amplitude of sinusoidal wall temperature variations strongly influence the fluid flow and temperature distributions, and consequently the local and overall heat transfer. At identical average temperature difference, applying a spatial variation in wall temperature at well-chosen phase angle can lead to significant heat transfer enhancement when compared to applying uniform wall temperatures at the cost of increased entropy generation.

Both the presence of the sphere packing and the nature of the spatial temperature variations along the vertical walls were found to have a large impact on the velocity and temperature of the fluid impinging on the hot and cold walls. This indicates that a variation in the arrangement of the sphere packing and in the diameter of the spheres can result in different local and overall heat transfer. Also, the spatial distances at which we obtain maximum and minimum local heat transfer will vary with the amplitude, wave length and phase angle arrangement of the wall temperature variations, especially *w.r.t* the location of large porosity regions close to the wall.

A study on the influence of the spatial frequency of the sinusoidal wall temperature variations on the local flow and temperature distribution, and hence on the heat transfer, is recommended for future investigation. We expect that cavities with sinusoidal wall temperature variations will behave like the cavities with con-

stant wall temperature in the limit of high spatial temperature variation frequencies, where the formation of local jet formation due to the interaction of the downward and upward flow close to the wall is expected to disappear.

Acknowledgments

This research was carried out under project number S41.5.14526a in the framework of the Partnership Program of the Materials innovation institute M2i (www.m2i.nl) and the Technology Foundation TTW (www.stw.nl), which is part of the Netherlands Organization for Scientific Research (www.nwo.nl). We would like to thank our industrial partner TATA Steel, The Netherlands, for continuous financial support and SURFsara for the support in using the Cartesius Computing Cluster (NWO File No.17178).

Appendix A. Validation of solver

To validate the steady-state solver "conjugateHeatSimpleFoam" in foam-extend-4.0, we simulate natural convection with conjugate heat transfer in a 2-D cavity illustrated in Fig. A1, discussed previously by [40,41].

Natural convection in a square $L \times L$ cavity with a $0.2 \times L$ thick conductive left wall is simulated to carry out the validation study. The conductive left wall is heated and the right side wall of the fluid-filled-cavity is cooled. The top and bottom walls are adiabatic.

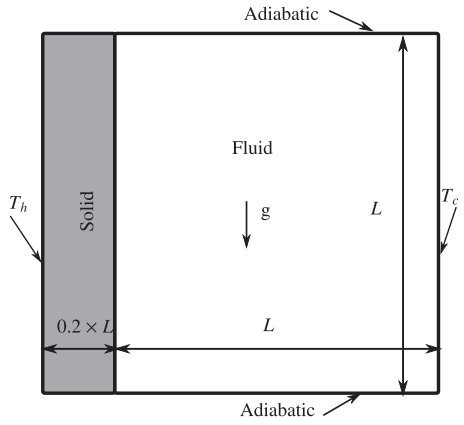

Fig. A1. Schematic representation of conjugate natural convection in a square enclosure with conducting wall.

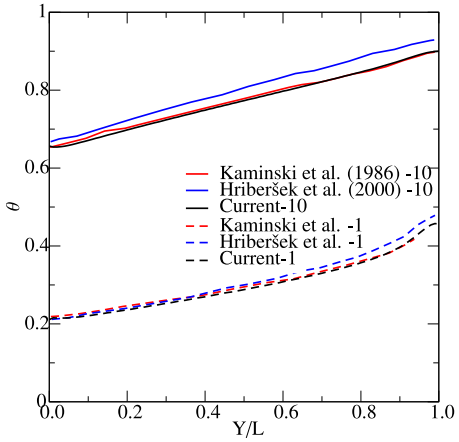

Fig. A2. Variation of non-dimensional temperature θ along the interface of solid and fluid region at $Gr = 10^7$ for $k_s/k_f = 1, 10$.

We used a 200×240 equidistant grid, with the solver and numerical settings as described in Section 2.2. We compare our results for the cases with the thermal conductivity ratio of the solid wall to the fluid, $k_s/k_f = 1, 10$, at a Grashof number, $Gr = 10^7$ and Prandtl number, $Pr = 0.7$, with the results reported in [40,41]. Our values of the non-dimensional temperature (θ) at the left solid-fluid interface reported in Fig. A2 are compared to the results reported in [40,41]. We obtain a fair agreement (differences in temperatures less than 5% and differences in heat flux less than 10%) with the results by Hriberšek and Kuhn [41], that were obtained with a boundary element method. We see a very good agreement (differences in temperatures less than 1% and differences in heat flux less than 3%) with the results by Kaminski [40] that were obtained with a steady-state control volume based finite difference method.

References

[1] D.J. Gunn, Transfer of heat or mass to particles in fixed and fluidised beds, Int. J. Heat Mass Transf. 21 (4) (1978) 467–476, doi:10.1016/0017-9310(78)90080-7.
[2] D.a. Nield, A. Bejan, Convection in Porous Media, 24, third ed., 2006.
[3] D.B. Ingham, I. Pop, Transport Phenomena in Porous Media II, 2002, doi:10.1007/BF00615200.
[4] A. Saxena, N. Agarwal, G. Srivastava, Design and performance of a solar air heater with long term heat storage, Int. J. Heat Mass Transf. 60 (2013) 8–16, doi:10.1016/j.ijheatmasstransfer.2012.12.044.
[5] S. Reichrath, T.W. Davies, Using CFD to model the internal climate of greenhouses: past, present and future, Agronomie 22 (1) (2002) 3–19, doi:10.1051/agro:2001006.
[6] H. Nazir, M. Batool, F.J. Bolivar Osorio, M. Isaza-Ruiz, X. Xu, K. Vignarooban, P. Phelan, Inamuddin, A.M. Kannan, Recent developments in phase change materials for energy storage applications: a review, Int. J. Heat Mass Transf. 129 (2019) 491–523, doi:10.1016/j.ijheatmasstransfer.2018.09.126.
[7] J. Zhang, X. Kan, Y. Shen, K.-C. Loh, C.-H. Wang, Y. Dai, Y.W. Tong, A hybrid biological and thermal waste-to-energy system with heat energy recovery and utilization for solid organic waste treatment, Energy 152 (2018) 214–222, doi:10.1016/j.energy.2018.03.143.
[8] P. Chao, H. Ozoe, S.W. Churchill, The effect of a non-uniform surface temperature on laminar natural convection in a rectangular enclosure, Chem. Eng. Commun. 9 (1–6) (1981) 245–254, doi:10.1080/00986448108911026.
[9] Y. Varol, H.F. Oztop, I. Pop, Numerical analysis of natural convection for a porous rectangular enclosure with sinusoidally varying temperature profile on the bottom wall, Int. Commun. Heat Mass Transf. 35 (1) (2008) 56–64, doi:10.1016/j.icheatmasstransfer.2007.05.015.
[10] W.-s. Fu, C.-c. Tseng, Y.-c. Chen, Natural convection in an enclosure with non-uniform wall temperature, Int. Commun. Heat Mass Transf 21 (6) (1994) 819–828. 0735-1933(94)00038-7
[11] Q. Deng, J. Chang, Natural convection in a rectangular enclosure with sinusoidal temperature distributions on both side walls, Numer. Heat Transf. Part A 54 (5) (2008) 507–524, doi:10.1080/01457630802186080.
[12] N.H. Saeid, Y. Yaacob, Natural convection in a square cavity with spatial sidewall temperature variation, Numer. Heat Transf. Part A 49 (7) (2006) 683–697, doi:10.1080/10407780500359943.
[13] N.H. Saeid, A.A. Mohamad, Natural convection in a porous cavity with spatial sidewall temperature variation, Int. J. Numer. Methods Heat Fluid Flow 15 (6) (2005) 555–566, doi:10.1108/09615530510601459.
[14] S. Sivasankaran, M. Bhuvaneswari, Natural convection in a porous cavity with sinusoidal heating on both sidewalls, Numer. Heat Transf. Part A 63 (1) (2013) 14–30, doi:10.1080/10407782.2012.715985.
[15] F. Wu, W. Zhou, X. Ma, Natural convection in a porous rectangular enclosure with sinusoidal temperature distributions on both side walls using a thermal non-equilibrium model, Int. J. Heat Mass Transf. 85 (2015) 756–771, doi:10.1016/j.ijheatmasstransfer.2015.02.039.
[16] T. Basak, R.S. Kaluri, A.R. Balakrishnan, Effects of thermal boundary conditions on entropy generation during natural convection, Numer. Heat Transf. Part A 59 (5) (2011) 372–402, doi:10.1080/10407782.2011.549075.
[17] T. Basak, S. Roy, T. Paul, I. Pop, Natural convection in a square cavity filled with a porous medium: effects of various thermal boundary conditions, Int. J. Heat Mass Transf. 49 (7–8) (2006) 1430–1441, doi:10.1016/j.ijheatmasstransfer.2005.09.018.
[18] A. Bejan, Entropy Generation Through Heat and Fluid Flow, Wiley, 1982.
[19] R.S. Kaluri, T. Basak, Entropy generation due to natural convection in discretely heated porous square cavities, Energy 36 (8) (2011) 5065–5080, doi:10.1016/j.energy.2011.06.001.
[20] M. Torabi, K. Zhang, G. Yang, J. Wang, P. Wu, Heat transfer and entropy generation analyses in a channel partially filled with porous media using local thermal non-equilibrium model, Energy 82 (2015) 922–938, doi:10.1016/j.energy.2015.01.102.
[21] S. Du, M.J. Li, Q. Ren, Q. Liang, Y.L. He, Pore-scale numerical simulation of fully coupled heat transfer process in porous volumetric solar receiver, Energy 140 (2017) 1267–1275, doi:10.1016/j.energy.2017.08.062.

[22] S. Bhardwaj, A. Dalal, S. Pati, Influence of wavy wall and non-uniform heating on natural convection heat transfer and entropy generation inside porous complex enclosure, Energy 79 (C) (2015) 467–481, doi:10.1016/j.energy.2014.11.036.
[23] I. Ataei-Dadavi, M. Chakkingal, S. Kenjereš, C.R. Kleijn, M.J. Tummers, Flow and heat transfer measurements in natural convection in coarse-grained porous media, Int. J. Heat Mass Transf. 130 (2019) 575–584, doi:10.1016/J.IJHEATMASSTRANSFER.2018.10.118.
[24] M. Chakkingal, S. Kenjereš, I. Ataei-Dadavi, M. Tummers, C.R. Kleijn, Numerical analysis of natural convection with conjugate heat transfer in coarse-grained porous media, Int. J. Heat Fluid Flow 77 (December 2018) (2019) 48–60, doi:10.1016/j.ijheatfluidflow.2019.03.008.
[25] I. Ataei-Dadavi, N. Rounaghi, M. Chakkingal, S. Kenjeres, C.R. Kleijn, M.J. Tummers, An experimental study of flow and heat transfer in a differentially side heated cavity filled with coarse porous media, Int. J. Heat Mass Transf. 143 (2019) 118591, doi:10.1016/j.ijheatmasstransfer.2019.118591.
[26] D.D. Gray, A. Giorgini, The validity of the Boussinesq approximation for liquids and gases, Int. J. Heat Mass Transf. 19 (5) (1976) 545–551, doi:10.1016/0017-9310(76)90168-X.
[27] H.G. Weller, G. Tabor, H. Jasak, C. Fureby, A tensorial approach to computational continuum mechanics using object-oriented techniques, Comput. Phys. 12 (6) (1998) 620–631, doi:10.1063/1.168744.
[28] J. Finn, S.V. Apte, Relative performance of body fitted and fictitious domain simulations of flow through fixed packed beds of spheres, Int. J. Multiphase Flow 56 (2013) 54–71, doi:10.1016/j.ijmultiphaseflow.2013.05.001.
[29] A. Zenklusen, S. Kenjereš, P.R. von Rohr, Vortex shedding in a highly porous structure, Chem. Eng. Sci. 106 (2014) 253–263, doi:10.1016/j.ces.2013.11.022.
[30] A. Zenklusen, S. Kenjereš, P.R. von Rohr, Mixing at high schmidt number in a complex porous structure, Chem. Eng. Sci. 150 (2016) 74–84, doi:10.1016/j.ces.2016.04.057.
[31] H. Rusche, H. Jasak, Implicit solution techniques for coupled multi-field problems Block Solution, Coupled Matrices, Presentation (2010) 22.
[32] I. Clifford, Block-coupled simulations using openfoam, Presentation (June) (2011) 1–47.
[33] A.M. Lankhorst, Laminar and Turbulent Convection in Cavities: Numerical Modeling and Experimental Validation, Technische Univ., Delft (Netherlands)., 1991 Ph.D. thesis.
[34] S.V. Patankar, Numerical Heat Transfer and Fluid Flow, Hemisphere Pub. Corp.; McGraw-Hill, Washington: New York, 1980.
[35] J. Patterson, J. Imberger, Unsteady natural convection in a rectangular cavity, J. Fluid Mech. 100 (1) (1980) 65, doi:10.1017/S0022112080001012.
[36] T. Basak, P. Gunda, R. Anandalakshmi, Analysis of entropy generation during natural convection in porous right-angled triangular cavities with various thermal boundary conditions, Int. J. Heat Mass Transf. 55 (17–18) (2012) 4521–4535, doi:10.1016/j.ijheatmasstransfer.2012.03.061.
[37] T. Basak, R.S. Kaluri, A.R. Balakrishnan, Entropy generation during natural convection in a porous cavity: effect of thermal boundary conditions, Numer. Heat Transf. Part A 62 (4) (2012) 336–364, doi:10.1080/10407782.2012.691059.
[38] G. Yang, J. Wu, L. Yan, Flow reversal and entropy generation due to buoyancy assisted mixed convection in the entrance region of a three dimensional vertical rectangular duct, Int. J. Heat Mass Transf. 67 (2013) 741–751, doi:10.1016/j.ijheatmasstransfer.2013.08.089.
[39] G. Yang, J. Wu, Entropy generation in a rectangular channel of buoyancy opposed mixed convection, Int. J. Heat Mass Transf. 86 (2015) 809–819, doi:10.1016/j.ijheatmasstransfer.2015.03.051.
[40] D. Kaminski, C. Prakash, Conjugate natural convection in a square enclosure: effect of conduction in one of the vertical walls, Int. J. Heat Mass Transf. 29 (12) (1986) 1979–1988, doi:10.1016/0017-9310(86)90017-7.
[41] M. Hriberšek, G. Kuhn, Conjugate heat transfer by boundary-domain integral method, Eng. Anal. Bound. Elem. 24 (4) (2000) 297–305, doi:10.1016/S0955-7997(00)00008-4.